Research article

Study on static and dynamic mechanical behavior of expansive soil modified by oyster shell powder

Wencan Jiao [a], Weizheng Zhou [b,**], Zhen Huang [b,c,*], Riyan Lan [a], Min Ma [b]

[a] *Guangxi Xinfazhan Communication Group Co., Ltd., Nanning, 530029, China*
[b] *School of Civil Engineering and Architecture, Guangxi University, Nanning, 530004, China*
[c] *State Key Laboratory of Featured Metal Materials and Life-cycle Safety for Composite Structures, Guangxi University, Nanning, 530004, China*

A B S T R A C T

To investigate the effect of oyster shell powder (OSP) on the static and dynamic properties of expansive soil, the mechanical properties of modified soil were obtained. Taking Ningming expansive soil as the research object, triaxial shear test, dynamic triaxial test and scanning electron microscope test were carried out on plain soil and 9 % expansive soil modified by oyster shell powder (ESMO). The results show that compared with plain soil, the effective cohesion of modified expansive soil with $d_{osp} < 1$ mm (ESMO ($d_{osp} < 1$ mm)) and $d_{osp} < 0.075$ mm (ESMO ($d_{osp} < 0.075$ mm)) is increased by 15.4 % and 32.8 %, respectively. Under cyclic loading, compared with plain soil, the plastic strain stability value of ESMO ($d_{osp} < 0.075$ mm) is reduced by 40.2 %, the pore water pressure stability value is reduced, and the stiffness is increased. The dynamic mechanical properties of ESMO ($d_{osp} < 1$ mm) showed the opposite trend. Through microscopic experimental analysis, the main reasons for this phenomenon are the particle size distribution, bonding form, and cementation of the two. The results can provide a theoretical basis for the practical application of ESMO and the establishment of constitutive model.

1. Introduction

Expansive soils have adverse engineering properties such as swelling-shrinkage, cracking, and over-consolidation, which are the main reasons for inducing cracking of buildings, instability of roadbeds or slopes, and damage to structures in expansive soil areas. At present, the treatment of expansive soil subgrades and slopes mainly adopts measures such as the replacement method, cushion method and core-spun method to limit the swelling-shrinking and cracking deformation of expansive soil [1]. However, these methods consume considerable manpower and material resources, and a large amount of borrowing and abandoning soil will cause environmental problems such as large-scale destruction of surface vegetation and loss of soil and water along railways [2].

To avoid such environmental problems, improving the engineering properties of expansive soil by adding various materials has become another effective method to treat expansive soil encountered in engineering. According to the mechanism of adding materials to improve the properties of expansive soil, these soil modification methods can be divided into chemical improvement, physical improvement, biological improvement and so on. In the chemical improvement method, lime [3–5], cement [6,7], coal fly ash [8],

expansive soil enzyme [9], ionic stabilizer [10] and other materials are added into the expansive soil. This method utilizes the reaction between the added material and the expansive minerals of the soil itself to generate stable minerals, thereby greatly reducing the expansion and contraction of expansive soil. For example, the addition of cement and lime will react in the soil to form calcium silicate, calcium aluminosilicate, calcium sulfate and other stable gel substances, and the reaction process will destroy the hydrophilic structure of the soil. Physical improvement mainly involves adding weathered sand [11,12] and gravel [13] to the expansive soil. Such methods generally do not change the original mineral composition of expansive soil. Instead, it improves the particle gradation of soil by adding materials, thus improving the shear strength of the soil. Biological improvement method utilizes the metabolic activity of microorganisms to promote mineral precipitation in soil, and dead microorganisms are used to fill the pores between particles to promote cementation between mineral particles, thereby improving the engineering properties of expansive soils [14]. The chemical improvement in the above methods can effectively improve the engineering properties of expansive soil, and the effect is fast. The defect is that it usually causes secondary pollution to the environment. Although the traditional physical improvement method of adding sand and gravel can improve the structural strength of the soil, it requires a considerable amount mined or purchased sand and gravel. Biological improvement is a green, environmentally friendly and energy-saving technique. However, this method has the disadvantage of high cost, and the related research is not in-depth enough, and the long-term stability and durability of the improved soil cannot be guaranteed. A method of improvement that combines environmental protection and improvement effects, while also being sufficiently economical, urgently needs to be proposed.

The recycling of solid waste protects the environment and contributes to the circular development of a green economy. Many scholars have used solid waste to improve the engineering properties of expansive soil, such as polypropylene fibre [15], waste coconut shell [16], sugarcane ash [17], coffee shell ash [18] and rice husk ash [19]. These kinds of materials have a certain improvement effect on expansive soil. The disadvantage is that some materials need to be incinerated before they can be used, while this process will causes air pollution. In addition, these materials are also easily corroded by soil, and the continuous improvement effect is poor. The availability of oyster shells, a solid waste in the food industry, has a rapidly increased in recent years. According to statistics, China's oyster production in 2019 alone was approximately 523,000 tons, an increase of approximately 9000 tons compared with 2018 [20]. A large number of oyster shells are discarded at will, occupying land resources, and the accumulation of solid waste has caused pollution of the soil and marine environment. In this regard, researchers have carried out a series of studies on the resource utilization of oyster shells, such as using oyster shells as adsorption material and soil amendments in sewage treatment and agricultural fields [21–24] and replacing some sand with oyster shell powder in building materials [25,26]. The main component of oyster shell is $CaCO_3$, which has excellent durability and stability [27]. Existing improvement measures for expansive soil will more or less incur certain pre-treatment costs. The pre-treatment methods of oyster shell powder are relatively simple, which can save the cost of improvement. Given this, OSP was used as a modification material for expansive soil in this study. Through this study, effective and diversified utilization of resources can be achieved, further promoting sustainable development.

The modified expansive soil will bear the cyclic load when used as subgrade filler. When the ESMO is used as filler, its plastic deformation under dynamic load should meet the requirements. Therefore, in order to ensure the stability of sbgrade under long-term cyclic load, its dynamic characteristics are studied. The research on the dynamic characteristics of modified expansive soil at home and abroad is in the development stage, and researchers such as Zhuang are interested in it. They used weathered sand [11,12], phosphorus tailings [28], and expanded polystylene [29] and other materials to carry out research. On this basis, the strength changes and
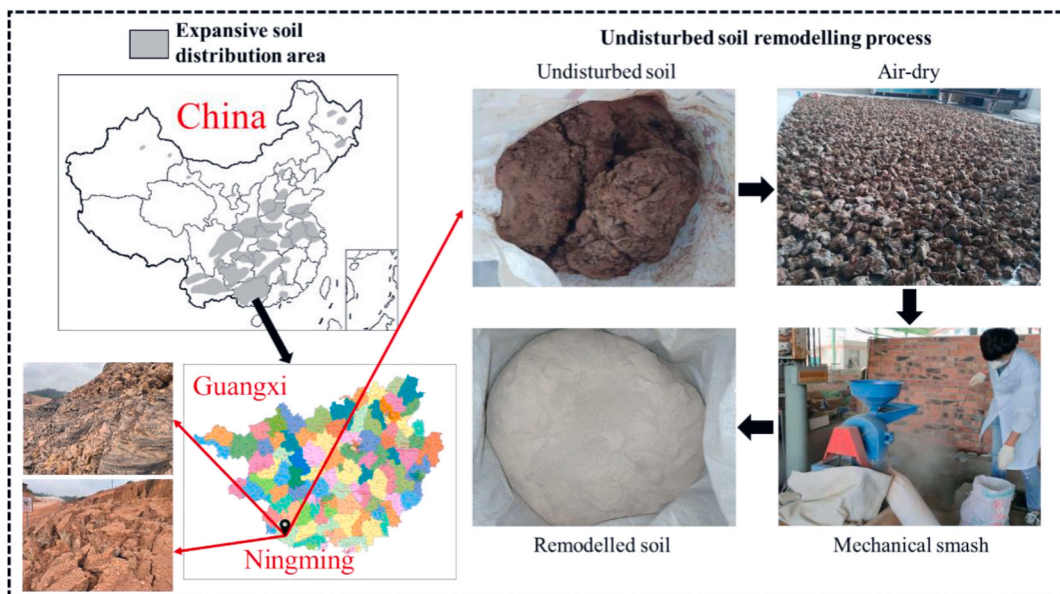

Fig. 1. Origin and remodelling process of expansive soil.

hysteresis curves of modified soil under different dynamic load conditions were obtained. The dynamic and static responses of expansive soil before and after modification are inconsistent. The dynamic load strength under cyclic load should be an essential factor affecting the strength parameters of modified soil. Previous studies have shown that adding oyster shell powder helps improve expansive soil's swelling, shrinkage, and cracking properties [30]. At the same time, the axial cumulative strain, damping ratio and dynamic resilient modulus are also improved to varying degrees [31]. However, the stress-strain relationship, pore pressure and other mechanical properties of ESMO were not explored.

Therefore, this study uses triaxial shear tests and dynamic triaxial tests to analyse the strength characteristics of ESMO under static and dynamic loads, including the stress−strain relationship, pore pressure-strain relationship and effective shear strength index of the modified soil under a static load. We studied the stress-strain relationship, pore pressure, hysteresis curve and dynamic elastic modulus of ESMO under different times of cyclic loading. The strengthening mechanism of the modified soil is explained from the microscopic point of view between expansive soil and OSP particles. By studying this process, we can gain a deeper understanding of the microstructure and properties of materials, thereby providing a theoretical basis for engineering applications. In addition, the mechanical parameters obtained from static and dynamic triaxial test results can provide theoretical basis for the establishment of constitutive models in numerical analysis.

2. Materials

2.1. Expansive soil

The test soil belongs to remolded soil. Fig. 1 shows the expansive soil's origin and remoulded soil's production. It comes from Ningming, Guangxi, China.

The free swelling rate refers to the expansion potential of soil in water in a loose state, which is the simplest and most intuitive method to distinguish the expansion category of expansive soil. Before the experiment, the expansive soil was sieved through 0.5 mm aperture and placed in a 105 °C constant temperature oven for 8 h. The test steps refer to the "Standard for geotechnical testing method" (GB/T 50123-2019) [32]. After the suspension was left to stand for 24 h, the height of the soil samples was recorded every 2 h. When the height of the soil sample does not change more than 0.2 ml in 6 h, the free expansion of the soil sample is considered to have reached a stable state (Fig. 2), and the free swelling rate of the soil is calculated according to equation (1).

$$\delta_{ef} = \frac{V_{we} - V_0}{V_0} \times 100 \tag{1}$$

where, δ_{ef} is the free swelling rate of the soil, in %; V_{we} is the volume of the soil sample after expansion and stabilization, in ml; V_0 is the initial volume of the soil sample, which is equivalent to the volume of the soil measuring cup and equal to 10 ml.

The free swelling ratio of the expansive soil used for the test was obtained as 82 % according to equation (1). According to the classification of expansive soil in the "Technical code for buildings in expansive soil regions" (GB 50112-2013) [33], the soil belongs to medium expansion potential expansive soil. The other basic physical properties of expansive soil were determined with reference to the "Standard for geotechnical testing method" (GBT 50123-2019) [32]. The results are shown in Table 1.

The mineral composition of the expansive soil was determined by X-ray diffraction (XRD) analysis, as shown in Fig. 3. It can be seen from the figure that the mineral composition of expansive soil mainly includes three hydrophilic expansive minerals, namely, illite, montmorillonite and kaolinite, mixed chlorite and quartz. This mineral composition gives expansive soil strong expansion properties [34].

Fig. 2. Free swelling rate test result.

Table 1
Basic physical properties of expansive soil.

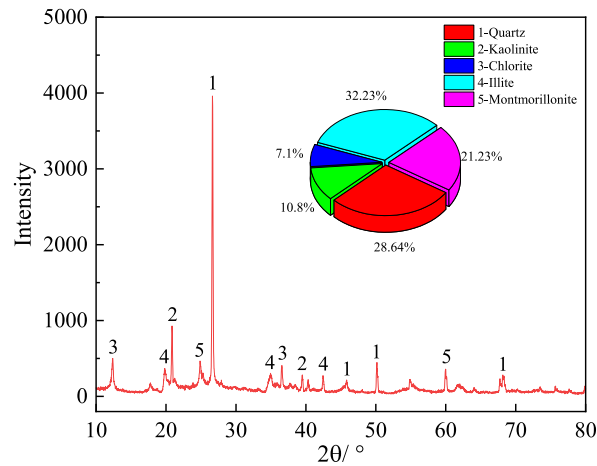| Natural moisture content/%	Optimum moisture content/%	Maximum dry density/ (g·cm^{-3})	Liquid limit W_L/%	Plastic limit W_P/%	Plasticity index I_P/%	Free swelling rate/%
35.67	18.3	1.61	60.1	22.2	37.9	82

Fig. 3. Mineral composition of expansive soil.

2.2. Oyster shell powder

The grey-white OSP used in this test is from Yangjiang, Guangdong Province, China. The calcination test of oyster shell powder was carried out, and the results are shown in Table 2. Chen's research showed that oyster shell powder has a mass loss of about 2.0–3.0 % between 230 and 600 °C, which is due to the decomposition of organic matter [35]. In addition, when oyster shell powder is calcined at a high temperature of 900 °C, calcium carbonate will decompose into calcium oxide and carbon dioxide. The mass loss caused by carbon dioxide escape can be converted to the mass of calcium carbonate before calcination. The mass loss due to decomposition of organic matter in oyster shell powder of each particle size is 2.5 %, and the mass of calcium carbonate in oyster shell powder can be calculated according to equation (2), and then the content of calcium carbonate can be obtained.

$$m_{CaCO_3} = \frac{m \times (1 - 0.025) - m_s}{M_{CO_2}} \times M_{CaCO_3} \tag{2}$$

where, M_{CO_2} is the molar mass of carbon dioxide, in g/mol; M_{CaCO_3} is the molar mass of calcium carbonate, in g/mol; m is the mass of the sample before calcination, in g; m_s is the remaining mass of the sample after calcination, in g; and m_{CaCO_3} is the mass of calcium carbonate contained in the sample, in g.

It can be seen from Table 2 that the calcium carbonate content of OSP is related to its particle size. The smaller the particle size, the more other ingredients in oyster shell powder. This indicates that some substances will not decompose at 900 °C and need to be further determined.
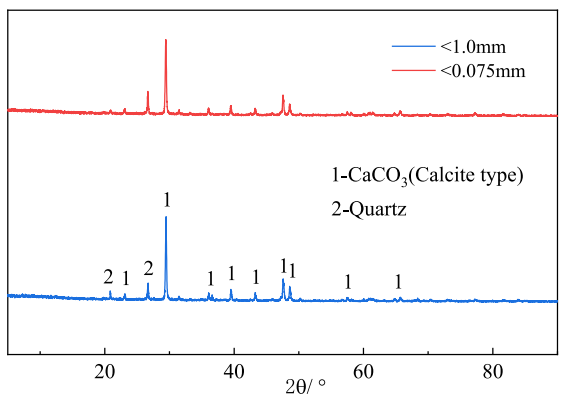
In this regard, we conducted an X-ray diffraction analysis of OSP and listed its phase composition under two particle sizes in Table 3. It can be concluded that the smaller the particle size of OSP, the more quartz, which is mainly due to a small amount of fine sand attached to the oyster shell. In the screening process, the smaller the OSP, the more fine sand will accumulate in the bottom layer.

It was determined by sieve analysis that 96.3 % of the oyster shell powder had a particle size of less than 1 mm, and 30.37 % of the oyster shell powder had a particle size of less than 0.075 mm. Three different particle specimens were obtained by passing the expansive soil through a sieve with a pore size of 1 mm and passing the oyster shell powder through a sieve with a pore size of 0.075 mm and 1 mm, respectively. The three specimens were then tested for particle size using a Malvern particle sizer (MS3000) and the results are shown in Fig. 4. It can be seen that there is a correlation between the particle size distribution of oyster shell powder and

Table 2
Calcination test results.

Grain size fraction /mm	Quality before calcination m/g	Quality after calcination m_s/g	Calcium carbonate quality m_{CaCO3}/g	Calcium carbonate content/%
<0.075	3.0007	1.8780	2.3811	79.35
<1	3.0008	1.6754	2.8418	94.70

Table 3
X-ray diffraction test results.

X-ray diffraction pattern		Particle size/mm	Mineral content/%	
			CaCO$_3$ (Calcite type)	Quartz
		<0.075	85.6	14.4
		<1	93.9	6.1

expansive soil, and the trend is as follows: oyster shell powder passed 1 mm sieve > expansive soil passed 1 mm sieve > oyster shell powder passed 0.075 mm sieve. Considering that the difference in the particle size distributions of the oyster shell powders passed through the 1 mm sieve and 0.075 mm sieve is mainly manifested in the content of particles > 100 μm, the large- and small-particle oyster shell powders mentioned in this paper are divided by the 100 μm particle size.

3. Test scheme

3.1. Determination of content and preparation of soil samples

Fig. 5 shows the results of the direct shear test and no-load expansion rate test of OSP modified expansive soil by Huang et al. [30], in which the content of OSP is 0 %, 3 %, 6 %, 9 % and 12 % respectively. The results show that the cohesion of the modified soil is the largest after 0–6 dry wet cycles when the content of OSP is 9 %. At the same time, increasing the content of OSP has no positive effect on its expansion rate. Therefore, the optimal content of OSP is 9 %. At the same time, considering that the particle size of the admixture will affect the improvement effect of the expansive soil [36], in this study, oyster shell powder was dried to constant weight after passing through the mesh screen with corresponding aperture, and mixed into expansive soil with the mass ratio of oyster:msoil = 9:91. The particle size of oyster shell powder was selected as $d_{osp} < 1$ mm and $d_{osp} < 0.075$ mm. These two groups were referred to as ESMO ($d_{osp} < 1$ mm) and ESMO ($d_{osp} < 0.075$ mm).

With reference to the "Standard for geotechnical testing method" (GBT 50123-2019) [32], the compaction method is selected to prepare samples. Remoulded soil was screened by 1 mm and dried sufficiently to prepare plain soil with 20 % moisture content and two kinds of ESMO ($d_{osp} < 1$ mm and $d_{osp} < 0.075$ mm). After being placed in the moisturizing bucket for 24 h, the compactness was controlled to 93 %, and the dry density was 1.50 g cm^{-3}. According to the formula, the remoulded soil with a total mass of $m = 1.5$
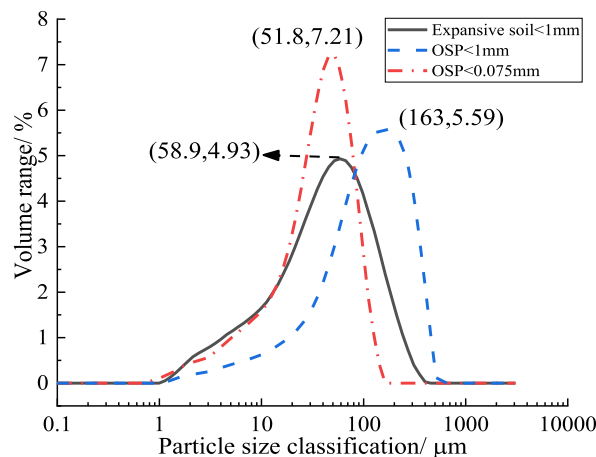

Fig. 4. Particle size distribution curve.

(a) Direct shear test
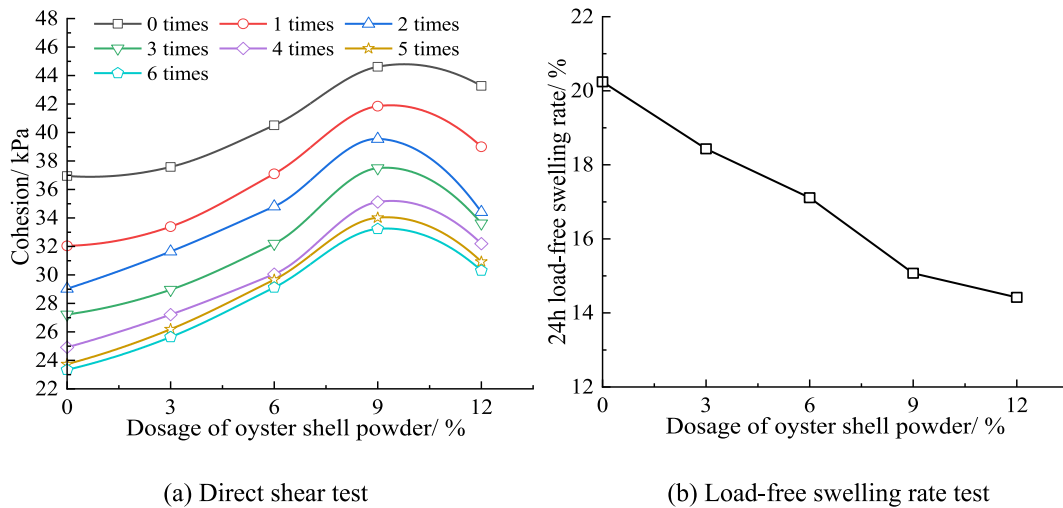
(b) Load-free swelling rate test

Fig. 5. Results of the direct shear test and load-free swelling rate test.

$(d/2)^2 \pi h(1+w)$ should be compacted into the cylinder coated with vaseline by five times (d is the diameter of the triaxial sample, h is the height). Table 4 shows the actual compaction parameters of triaxial specimens. Due to the high viscosity of expansive soil, it is necessary to wrap a layer of filter paper around the sample and put it into the vacuum pump for saturation. Triaxial tests can be carried out after saturation and immersion in water for 24 h.

3.2. Triaxial shear test

Triaxial shear tests were performed on a GDS Triaxial Testing System (GDSTTS). The equipment mainly applies axial stress directly through the hydraulic control hammer at the base of the pressure chamber and controls the stress path by the radial stress loading. The height of a corresponding sample was 76 mm, and the diameter was 38 mm. When installing the sample, 4 filter paper strips were added around the sample to speed up the process of back pressure saturation and consolidation. When the pore pressure coefficient B > 0.98, the back pressure saturation of the sample is completed, and then isotropic consolidation is carried out. The consolidation confining pressures were 75, 125, 200, and 300 kPa, and undrained shearing was performed after consolidation was completed. The shear stress path is as follows: the confining pressure remains unchanged, the axial pressure increases, and the test is terminated when the axial strain reaches 20 %. Table 5 shows the triaxial shear test scheme.

3.3. Dynamic triaxial test

The dynamic triaxial tests were realized with a GDS Dynamic Triaxial Testing System (GDS-DYNTTS). The system applies the axial load through a pneumatic servo control system, which can realize stress- and strain-controlled cyclic loading tests using the advanced loading module and dynamic loading module of this system. The height of a corresponding specimen was 100 mm, and the diameter

Table 4
Compaction parameters of triaxial specimen.

Sample number	Test types	Content of oyster shell powder/%	Particle size of oyster shell powder/mm	Actual moisture content/%	Actual dry density/ $(g \cdot cm^{-3})$
A1	Triaxial shear test	0	/	20.07	1.52
A2		0	/	20.07	1.51
A3		0	/	20.07	1.52
A4		0	/	20.07	1.51
B1		9	<1	20.35	1.50
B2		9	<1	20.35	1.49
B3		9	<1	20.35	1.51
B4		9	<1	20.35	1.51
C1		9	<0.075	20.82	1.52
C2		9	<0.075	20.82	1.52
C3		9	<0.075	20.82	1.51
C4		9	<0.075	20.82	1.52
D1	Dynamic triaxial test	0	/	20.05	1.50
D2		9	<1	20.21	1.51
D3		9	<0.075	20.45	1.51

Table 5
Triaxial shear test scheme.

Sample number	Content of oyster shell powder/%	Particle size of oyster shell powder/mm	Confining pressure/kPa	Strain control rate/(%/min)
A1	0	/	75	0.05
A2	0	/	125	0.05
A3	0	/	200	0.05
A4	0	/	300	0.05
B1	9	<1	75	0.05
B2	9	<1	125	0.05
B3	9	<1	200	0.05
B4	9	<1	300	0.05
C1	9	<0.075	75	0.05
C2	9	<0.075	125	0.05
C3	9	<0.075	200	0.05
C4	9	<0.075	300	0.05

was 50 mm. When installing the specimen, 5 filter paper strips were added around the sample to speed up the process of back pressure saturation and consolidation. After the sample was saturated by back pressure and the pore pressure coefficient B > 0.98, isotropic consolidation was carried out, and the consolidation confining pressure was 125 kPa. Traffic and wave, earthquake, mechanical and other dynamic loads can be simulated by cyclic triaxial load test [37]. By comparing the similarity of multiple forms of dynamic load loading waveforms with train loads, Zhang [38] pointed out that bias sinusoidal waves can better represent the realism of train loads. According to the measured data obtained by Kong et al. [39], the additional stress generated in foundation soil during the running of a train is in the range of 10–50 kPa. Therefore, the offset sine wave shown in Fig. 6 is used in this study as the waveform of the applied dynamic load. The dynamic triaxial test scheme is shown in Table 6. The train load is transient, and the modified soil is often buried shallowly as subgrade filler, so no drainage is conducted during the loading process. The test instruments and procedures of the triaxial shear test and the dynamic triaxial test are similar, as shown in Fig. 7. Fig. 8 is the research flowchart of this study.

4. Results and analysis

4.1. Static mechanical behaviour

4.1.1. Stress-strain relationship

Fig. 9(a and b) shows the stress-strain relationship curves of plain soil and modified soil under different confining pressures, where q is the deviator stress $\sigma_1 - \sigma_3$ and ε_1 is the axial strain. Test group A is plain soil, test group B is ESMO ($d_{osp} < 1$ mm), and test group C is ESMO ($d_{osp} < 0.075$ mm).

Fig. 9(a–d) shows that the development trends of the stress-strain curves of the plain soil and the modified soil under different confining pressures are consistent. For experimental group A, the stress-strain curve exhibits three stages: (a) When the stress is small, the stress-strain curve is approximately a straight line and is in the stage of elastic deformation; (b) With the increase in stress, the stress-strain curve gradually deviates from the straight line and turns into nonlinear growth, and the proportion of plastic deformation increases; (c) When the stress reaches the peak point, the stress-strain curve shows a downwards trend, the plastic deformation increases rapidly, and the load that the sample can bear decreases. This shows that experimental group A exhibited obvious strain softening properties. For test groups B and C, the stress-strain curve also experienced three stages. The first two stages were consistent with those of test group A, and the third stage showed that the stress gradually stabilized with increasing strain, corresponding to obvious strain hardening properties. Before the axial strain of test groups B and C reached 20 %, there was still no obvious peak point of stress. From the stress-strain curves of samples C2 and C3, it can be seen that the stress had a certain downwards trend after a large strain. Considering that the calculation of the deviator stress by the instrument was distorted after a large strain, generally, if there was
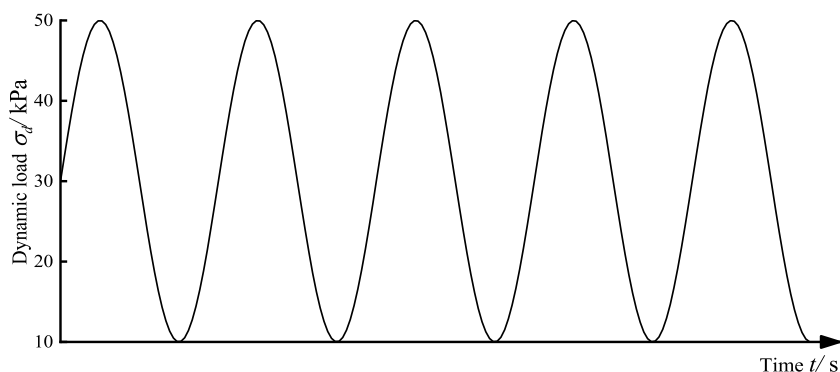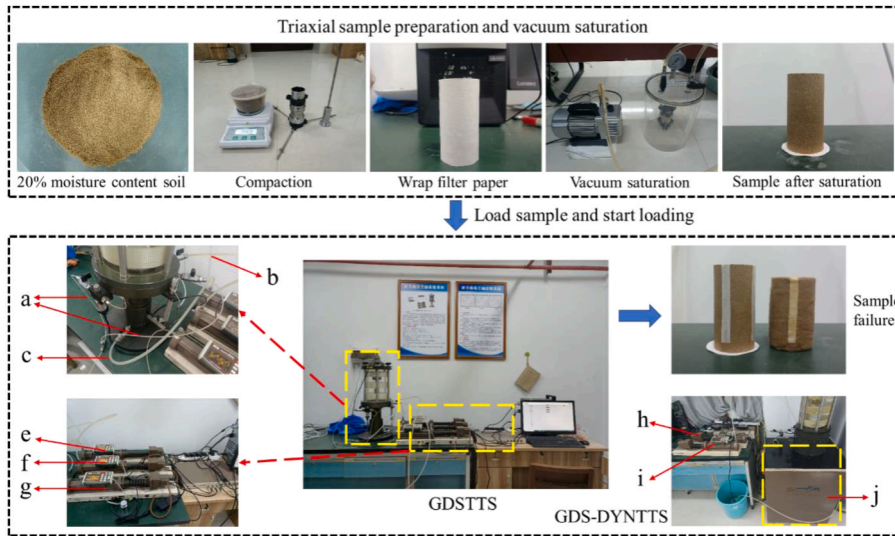

Fig. 6. Loading curve of cyclic loading.

Table 6
Dynamic triaxial test scheme.

Sample number	Content of OSP/%	Particle size of OSP /mm	Static deviatoric stress/kPa	Amplitude/ kPa	Frequency/ Hz	Confining pressure/kPa	Number of cycles
D1	0	/	30	20	1	125	20000
D2	9	<1	30	20	1	125	20000
D3	9	<0.075	30	20	1	125	20000

Note: a. Back pressure controller connection; b. Confining pressure controller connection; c. Axial pressure

controller connection; e. Axial pressure controller; f & i. Confining pressure controller; g & h. Back pressure

controller; j. Pneumatic servo control system

Fig. 7. Triaxial test equipment and process.

no stress peak before 15 % strain, strain hardening could be assumed.

Generally, for strain-softening soils, the peak point of deviator stress is taken as the failure deviator stress. For strain hardening soil, the deviator stress corresponding to 15 % axial strain is taken as the failure deviator stress. It can also be seen from Fig. 9 that the comparison relationship between the stress-strain curves of the three test groups are consistent under different confining pressures. The stress-strain curve of test group C plots highest in the graph, indicating that the failure deviator stress of ESMO ($d_{osp} < 0.075$ mm) is the largest among the three test groups. The stress-strain curves of test groups of A and B intersect, and the intersection points are near the position of 15 % axial strain. The deviator stress in the front section is A > B, and the deviator stress in the rear section is A < B. There is no significant difference in the deviatoric stress at failure between the two groups.

4.1.2. Pore pressure-strain relationship

Fig. 10 shows the pore pressure-strain relationship curves of plain soil and modified soil under different confining pressures, where Δu is the excess pore water pressure during the shearing process and ε_1 is the axial strain.

Fig. 10(a–d) shows that the pore pressure-strain curves of the plain soil and modified soil under different confining pressures have the same trend, which can be divided into three stages: (a) When the axial strain is small, the pore pressure increases linearly with the strain; (b) When the strain increases to approximately 1 %, the pore pressure increases nonlinearly with increasing strain, and the growth rate gradually slows and finally peaks; (c) When the pore pressure reaches the peak point, the pore pressure linearly decreases with increasing strain. The test was terminated after reaching 20 % strain, and the pore pressure still had a downwards trend at this time.

It can also be seen from Fig. 10 that under different confining pressures, there are certain differences in the comparison relationship of the pore pressure-strain curves between plain soil and the two kinds of modified soil. Under each confining pressure, the pore pressure-strain curve of test group B plots highest in the graph. The pore pressure difference of test group A and C has an obvious law,
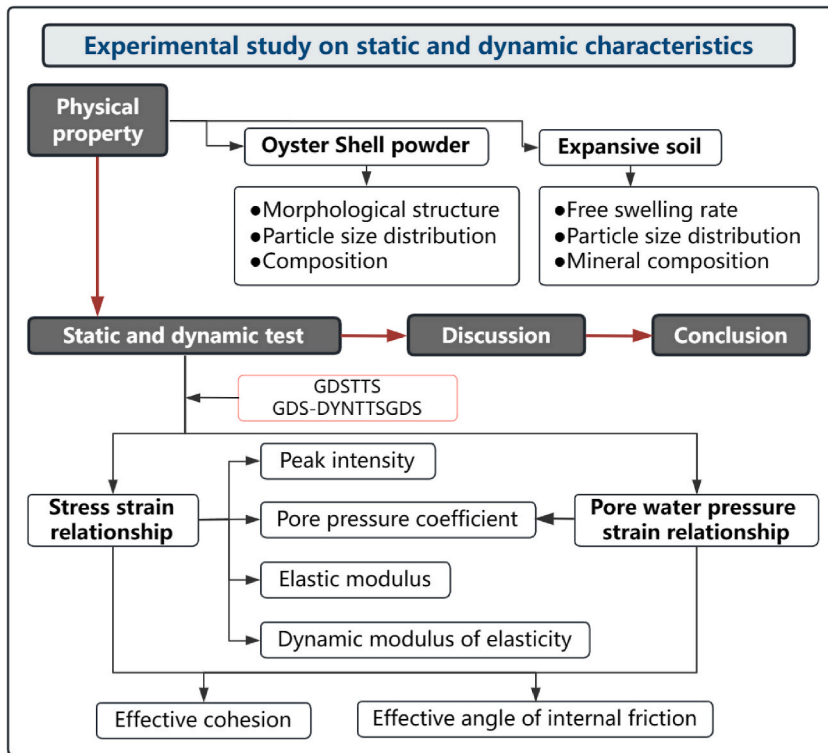
Fig. 8. Flowchart of research.

which shows that the pore pressure difference between them gradually increases with the increase of confining pressure. In general, the pore pressure of the ESMO ($d_{osp} < 0.075$ mm) was the smallest among the three, indicating that the effective stress borne by the soil was better than plain soil under the same axial strain.

4.1.3. Shear strength

In this study, the Mohr-Coulomb failure criterion was used to determine the shear strength envelopes and shear strength indexes of the three soils. Since the change in pore pressure could be measured in the triaxial shear tests, the effective stress-shear strength equation (Eq. (3)) was used here:

$$\tau_f = c' + \sigma' \tan \varphi' \tag{3}$$

In the formula, τ_f is the shear strength, σ' is the effective normal stress on the shear failure plane, c' is the effective cohesion, and φ' is the effective angle of internal friction. Relying on the effective principal stresses σ'_3 and σ'_1 when the failure deviation stress is reached, the Mohr circle of the limit state was plotted in the $\sigma' - \tau$ plane, the principal stress line of effective stress failure K'_f was plotted through the Mohr circle vertex of the limit state under each confining pressure, and the vertex coordinates are $\sigma' = \frac{\sigma'_1 + \sigma'_3}{2}$ and $\tau = \frac{\sigma'_1 - \sigma'_3}{2}$. The K'_f line and fitting line equations of test groups A, B and C are shown in Fig. 11(a–c).

The shear strength envelope is the common tangent of the Mohr circle of the limit state under each confining pressure. Ideally, there is a geometric relationship between the K'_f line and the shear strength envelope on the $\sigma' - \tau$ plane, as shown in Fig. 12.

Assuming that the inclination of the K'_f line is α'_f and that the intercept is a', then the effective angle of internal friction φ' and the effective cohesion c' of the soil mass have the following relationship with α'_f and a':

$$\varphi' = \sin^{-1} \tan \alpha'_f \tag{4}$$

$$c' = \frac{a'}{\tan \alpha'_f} \cdot \tan \varphi' = \frac{a'}{\cos \varphi'} \tag{5}$$

From Eqs. (4) and (5), the effective shear strength indexes c' and φ' of the three kinds of soil masses were calculated, which are listed in Table 7:

Table 7 shows that the effective angle of internal friction of plain soil, ESMO ($d_{osp} < 0.075$ mm) and ESMO ($d_{osp} < 1$ mm) were not
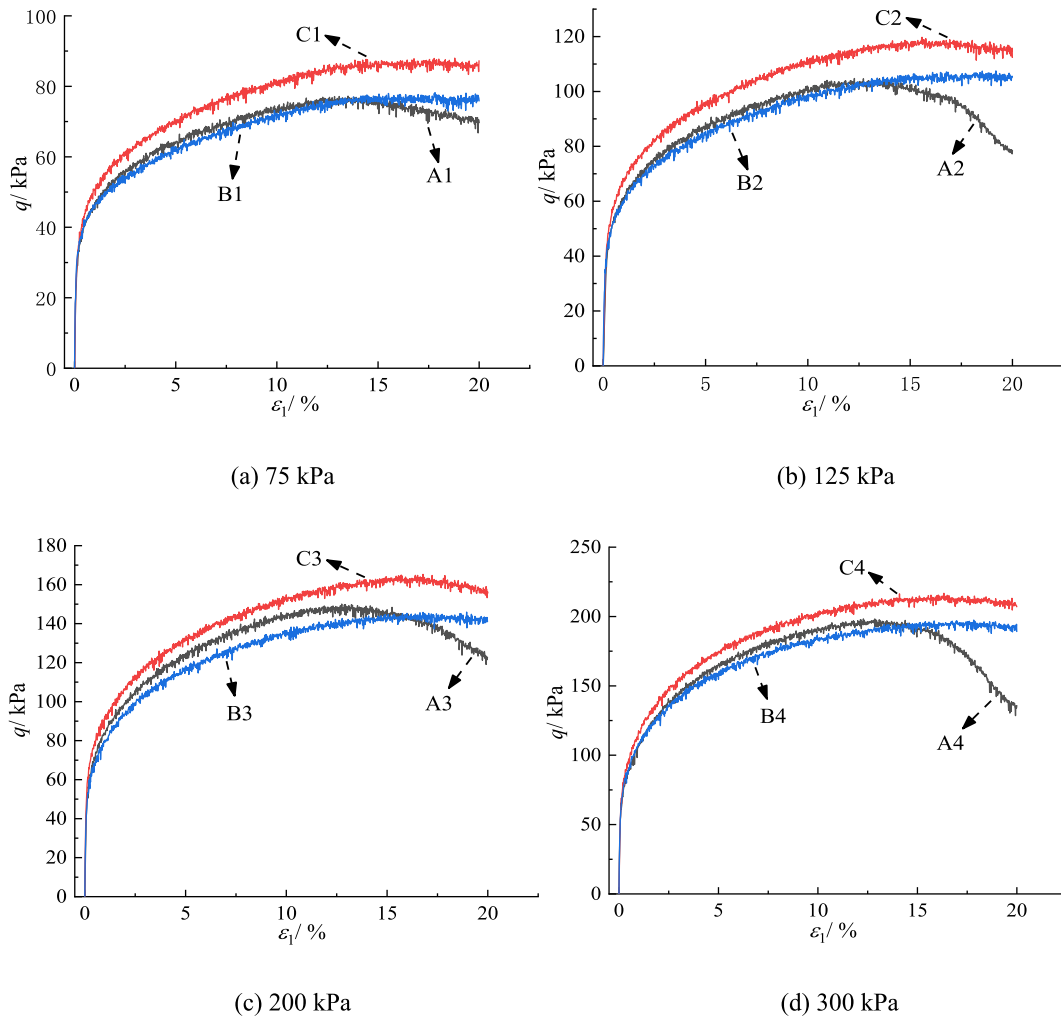
(a) 75 kPa

(b) 125 kPa

(c) 200 kPa

(d) 300 kPa

Fig. 9. Stress-strain relationship curve.

much different. It shows that for the whole sample, adding OSP with different particle sizes has no significant effect on the total utility of sliding and interlocking action within soil particles. Compared with plain soil, the effective cohesion of ESMO ($d_{osp} < 1$ mm) increased by 15.4 %, and the effective cohesion of ESMO ($d_{osp} < 0.075$ mm) increased by 32.8 %, which indicates that the addition of oyster shell powder can significantly improve the static properties of expansive soil. Thus, OSP with smaller particle size shows better improvement performance.

4.2. Dynamic mechanical behaviour

4.2.1. Axial strain-number of vibration loads relationship

Fig. 13 shows the axial strain-number of vibration loads relationship curves, where D1 is plain soil, D2 is ESMO ($d_{osp} < 1$ mm), and D3 is ESMO ($d_{osp} < 0.075$ mm).

Fig. 13 shows that the variations in the axial strain of the three soils with the number of vibration loads are consistent. At the beginning of the test, the internal pores of the soil were obviously compacted by the external force, and the rate of axial strain accumulation was fast. With the increase in the number of vibration loads, a sample was gradually compacted, and the axial strain gradually became stable after 5000 vibration loads. The plastic strains of D1, D2, and D3 at 20,000 vibrations were 1.12 %, 1.82 %, and 0.67 %, respectively. Under the same conditions, the plastic strain stability value of ESMO ($d_{osp} < 0.075$ mm) was 40.2 % lower than that of plain soil, indicating that the addition of small particles of OSP can greatly improve the ability of expansive soil to resist plastic deformation. The plastic strain of ESMO ($d_{osp} < 1$ mm) was larger than plain soil. Obviously, the addition of OSP with a larger particle size was not conducive to the stability of the soil structure of expansive soil under long-term cyclic loading.
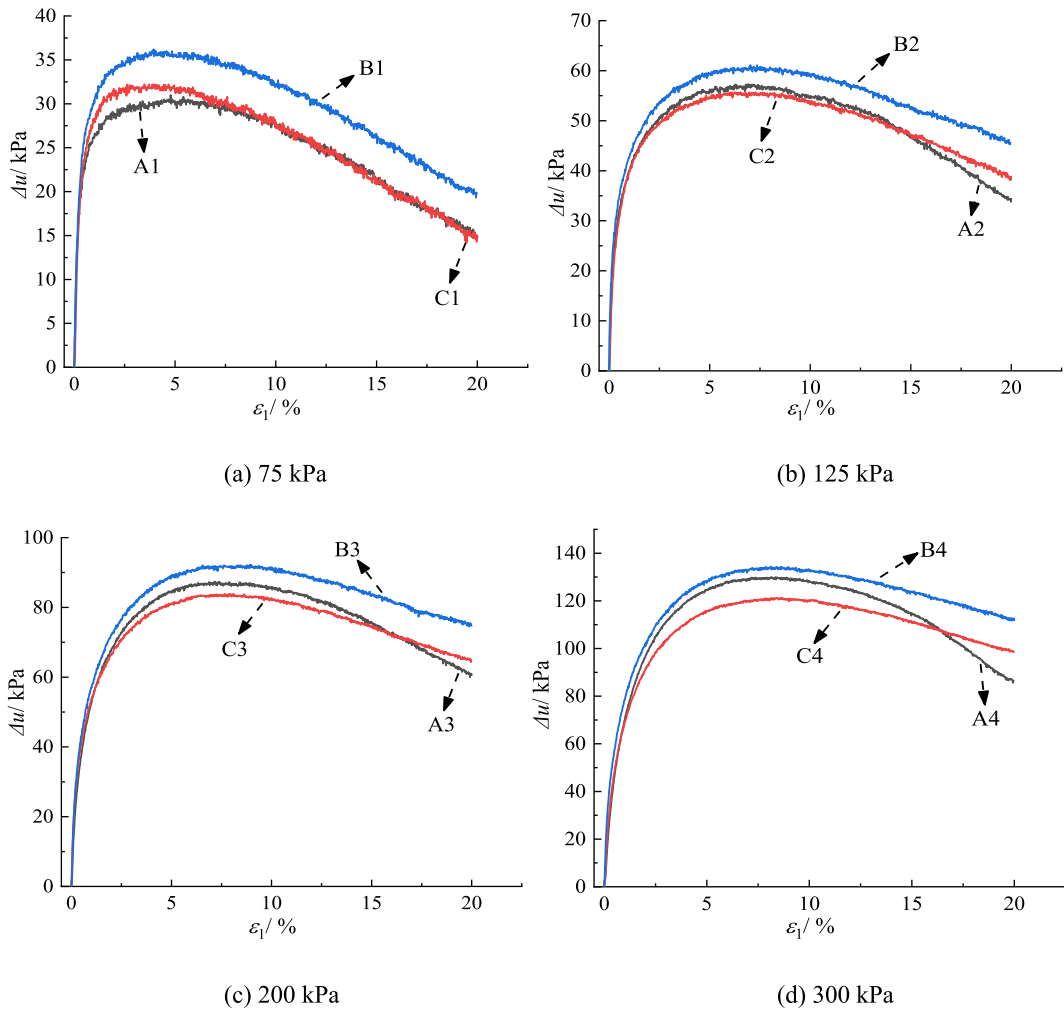
(a) 75 kPa

(b) 125 kPa

(c) 200 kPa

(d) 300 kPa

Fig. 10. Pore pressure-strain relationship curve.

(a) Plain soil

(b) ESMO (d_{osp} <1 mm)
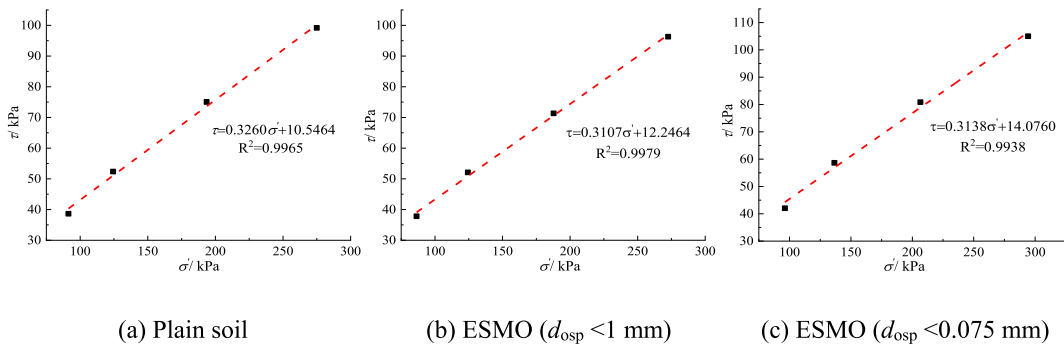
(c) ESMO (d_{osp} <0.075 mm)

Fig. 11. $K_f^{'}$ fitting curves.

4.2.2. Pore pressure-number of vibration loads relationship

Fig. 14 shows the excess pore water pressure-number of vibration loads curve of plain soil and modified soil. The samples represented by D1, D2 and D3 are the same as above. Under the action of cyclic loading, the pore pressure also fluctuated sinusoidally within one cycle. After the pore pressures of D1, D2, and D3 increased to a stable level, the peak-to-peak values of a cycle (The difference between the maximum pore pressure and the minimum pore pressure in a cycle) were 7.1 kPa, 6.3 kPa, and 7.5 kPa, respectively, and the difference between the three pore pressures was small after stabilization, thus Fig. 14 shows only the pore
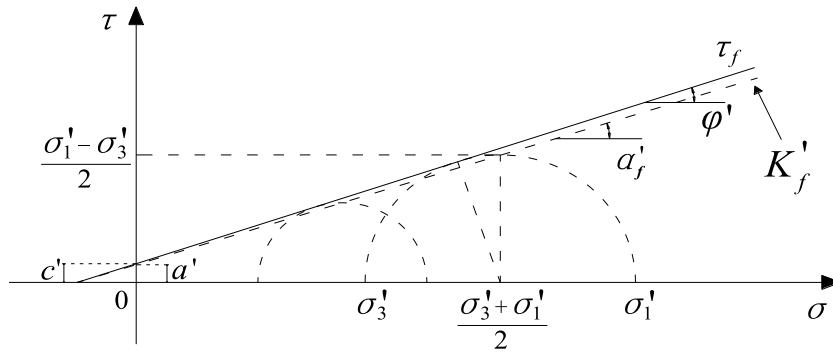
Fig. 12. The relationship among a', a'_f, c' and φ'.

Table 7
Effective shear strength indexes.

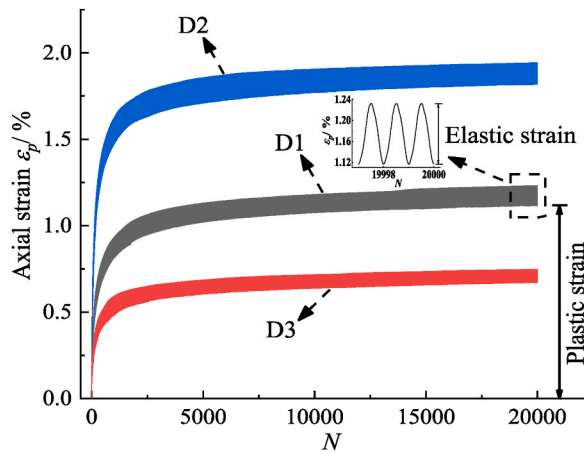| Number	Content/%	Particle size/mm	c'/kPa	φ'/(°)
A	0	/	11.16	19.03
B	9	1	12.88	18.10
C	9	0.075	14.82	18.29

Fig. 13. Axial strain-number of vibration loads relationship curve.

pressure accumulated in each cycle (minimum pore pressure in a single cycle). Fig. 14 shows that the pore pressure accumulation rate of ESMO (d_{osp} < 0.075 mm) was slower than that of plain soil, and the final stable pore pressure was also smaller. In contrast, for ESMO (d_{osp} < 1 mm), a larger excess pore pressure corresponds to a decrease in effective stress on the soil skeleton and then cause a decrease in strength [40].

4.2.3. Stress-strain hysteretic loop characteristics and dynamic elastic modulus

Fig. 15 shows the overall trend of the hysteretic loop of plain soil and ESMO. The hysteretic curves of the three soils are similar, and the change trend is consistent. In the first few cycles, the hysteresis loop is not closed, indicating that the accumulation of permanent plastic strain is large. With the increase in the number of cycles, the hysteresis loop gradually closed and narrowed, indicating that the accumulated axial strain was decreasing. Obviously, there are differences in the hysteretic loop area S and the major axis slope k among the three soils, which are discussed separately below.

The energy dissipation characteristics of soil can be reflected by the area S of hysteresis loop (non closed hysteresis loop is calculated by connecting the head and tail straight line of the curve). Fig. 16 shows the relationship between the number of cycles and S. With the increase in the number of cycles, the S of the three kinds of soil samples first decreased sharply, and then the decreasing trend gradually slowed down. The stability of plain soil is faster than ESMO. After 20000 cycles of cyclic loading, ESMO still has a downward trend. The overall size relationship of the S values of the three soils is D2 > D1 > D3, indicating that the energy dissipation of ESMO (d_{osp} < 0.075 mm) is lower than that of plain soil and that the energy dissipation of ESMO (d_{osp} < 1 mm) is the higher.
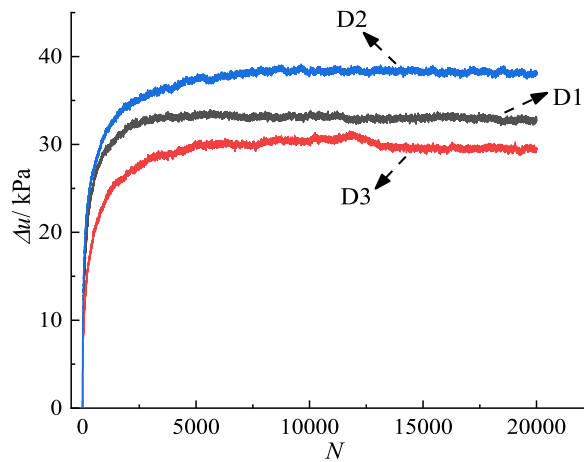
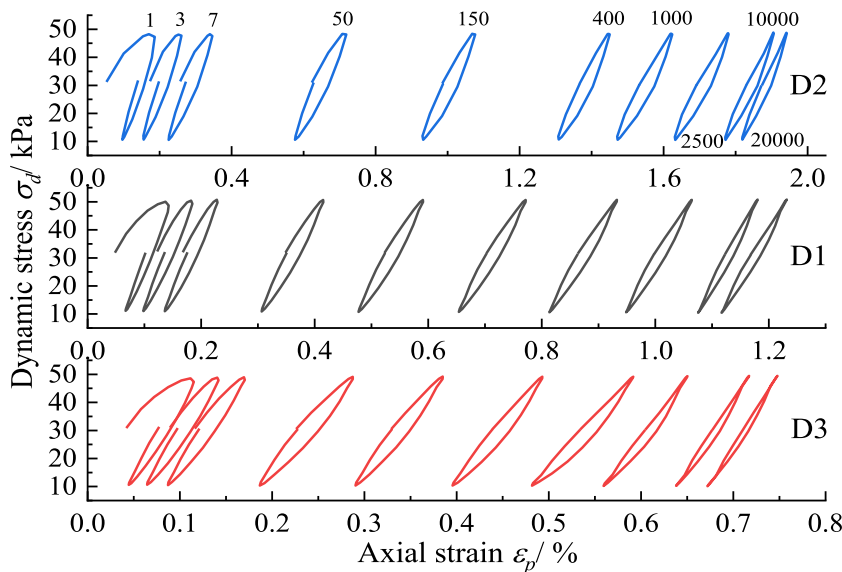**Fig. 14.** Cumulative pore pressure-number of vibration loads curve.

Fig. 15. Shape and characteristics of the hysteretic loops.

The slope k of the major axis of the hysteretic loop reflects the stiffness of the soil, and k is the ratio of the difference between the maximum and minimum values of the dynamic stress of the axial hysteretic loop and the corresponding dynamic strain difference, which is defined as the dynamic elastic modulus E_d. Fig. 17 shows the relationship between E_d and the number of vibration loads of the three soils. E_d sharply decreases in the early stage of cyclic action and then develops slowly. The overall size relationship of the three soils is D3 > D1 > D2, indicating that ESMO ($d_{osp} < 0.075$ mm) is more stiff than plain soil and that ESMO ($d_{osp} < 1$ mm) is less stiff.

5. Discussion

5.1. Microscopic mechanism

From the above test results, the static and dynamic mechanical properties of ESMO ($d_{osp} < 0.075$ mm) significantly improved. The static mechanical properties of ESMO ($d_{osp} < 1$ mm) were improved, while the dynamic mechanical properties were greatly deteriorated. In order to further explore the mechanism of oyster shell powder modified expansive soil, the oyster shell powder and expansive soil were tested by scanning electron microscope (SEM).

It can be seen from Fig. 18(a and b) that the oyster shell powder, after mechanical crushing, is mainly flake, and there are also flocculent morphological structures. Due to the stability of calcium carbonate, this morphological structure will not be easily changed due to the invasion of water. The microstructure of compacted plain expansive soil samples exhibits a layered structure with edge-edge combination and surface-surface combination. On the whole, the direction of this locally highly oriented structure is inconsistent at
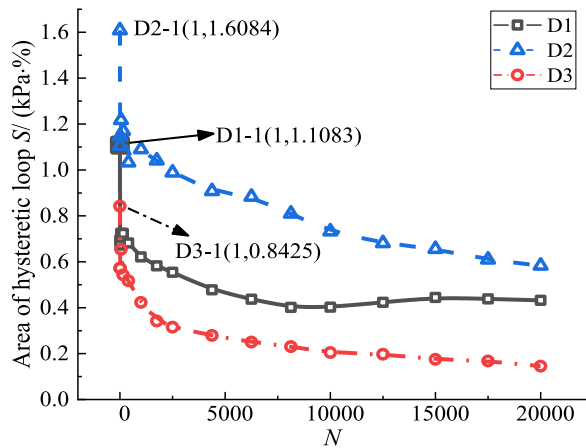
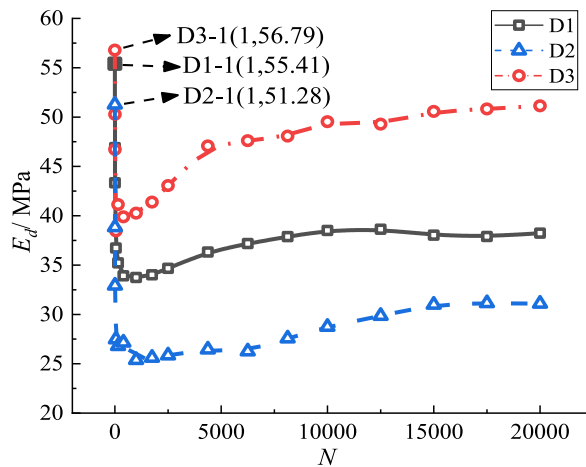**Fig. 16.** Hysteretic loop area-number of vibration loads relationship curve.

Fig. 17. Elastic modulus-number of vibration loads relationship curve.

different positions, resulting in a very complicated combination of expansive soil particles mixed with oyster shell powder after compaction.

Fig. 19(a and b) shows one of the combinations of OSP and expansive soil observed in the SEM test. It can be seen from Fig. 19(a and b) that incorporating oyster shell powder will prevent and weaken the parallelization of the expansive soil layer structure and form a disturbed layered structure. Due to the appearance of this structure, the strength of ESMO is improved, which gives it better performance under cyclic load. The large specific surface area of oyster shell powder of 1.8 m^2/g can bond the expansive soil particles well, and the cementing effect of calcium carbonate, the main component of oyster shell powder, further improves its bonding ability to the soil particles [31]. The smaller the particle size of OSP, the larger the specific surface area, which can give full play to the cementation of $CaCO_3$. Under the action of load, the interaction force between oyster shell powder and expansive soil particles is more significant than that between plain soil particles, and the overall cohesion of modified soil is enhanced. With the decrease of OSP particle size, the soil strength increased more obviously. The change of soil internal friction angle before and after modification may be caused by the physical, mechanical occlusion or some chemical reactions between oyster shell powder and expansive soil.

Fig. 20 shows another form of action between the modified material and expansive soil particles. The flake OSP contacts with soil particles to form a similar "bridge" structure. Because of the existence of this layer structure, the speed of soil particles developing into layered structures under the compression of cyclic load is effectively slowed down to maintain a more irregular state. From the above experiments, it can be concluded that this structure requires oyster shell particle size in an appropriate state. Too large particle size will cause the pores between the modified soil particles to become more prominent, the skeleton to become loose, and the pore pressure to become more prominent, which will deteriorate the mechanical performance of the modified soil. The increase in the hysteresis loop area reflects the increase in energy consumption of soil under dynamic action [41]. The dynamic wave must pass through multiple conductions between pores and particles, which consumes more energy.

In addition to the above reasons, the improvement effect of OSP on expansive soil may also be due to a series of physical and chemical changes between them. Inspired by the research of Amaludin et al. [42], the physical chemistry and microstructure of soil
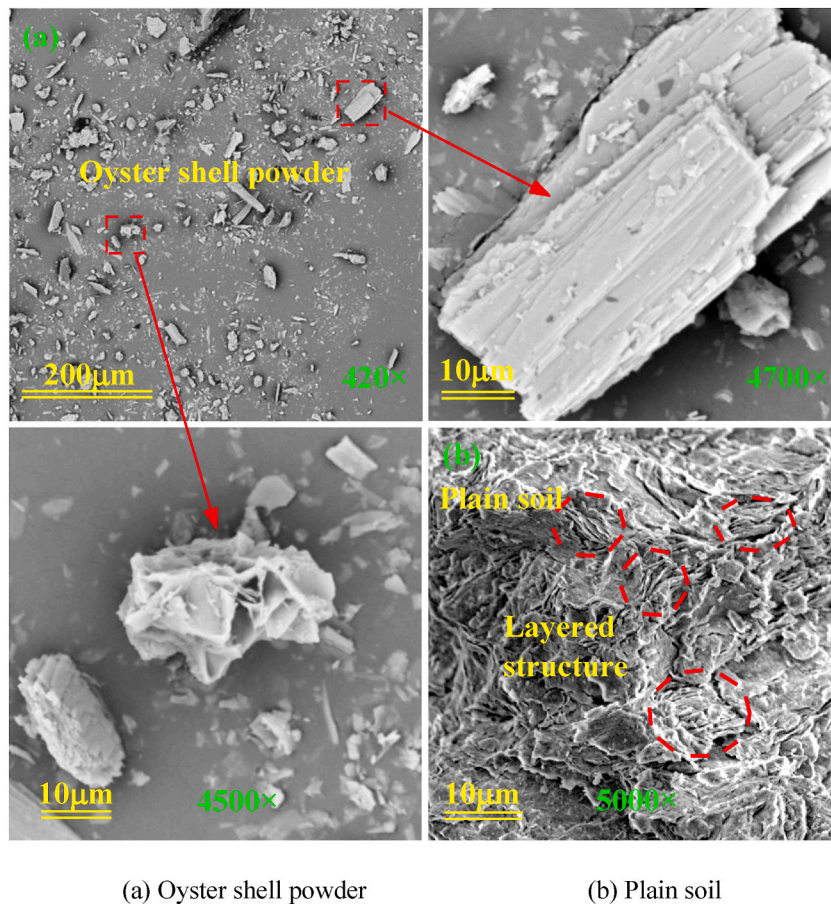
(a) Oyster shell powder   (b) Plain soil

Fig. 18. Microstructure of oyster shell powder and plain soil.

stability are often closely related. The outer cuticle of oyster shell powder interferes with the ability of calcium carbonate to achieve its full function. However, there are many cross sections that allow calcium carbonate to maintain direct contact with expansive soil and water. Some scholars have shown that [43], fly ash reacts with straw ash, laterite soil, and alkaline solutions to generate alumina-silica binders in fly ashbased geopolymer binders without cement. Therefore, the micro calcium ion precipitated from calcium carbonate in water and the change of pH value of pore water may cause further physical and chemical reactions.

5.2. Prospect and application

The results show that ESMO has the prospect of practical engineering application, because the oyster shell powder with particle size less than 0.075 mm accounts for 30.37 % of the OSP used in this research, and the particle size control is feasible in practical operation. In addition, the mechanical parameters obtained from the static and dynamic triaxial test results can provide a theoretical basis for the establishment of constitutive models in numerical analysis.

In road engineering, ESMO can be used to prepare stabilized soil base material to improve the bearing capacity and stability of the road. In construction engineering, ESMO can be used to improve soil properties, improve the stability of the foundation, and reduce settlement and cracking problems. In geological engineering, ESMO can strengthen soft foundations and prevent landslides. In short, the research results of ESMO have a wide range of applications in engineering. With the deepening of related research, the engineering application of oyster shell powder modified expansion will be more and more widely and will make more remarkable contributions to environmental protection.

6. Conclusion

(1) In terms of static mechanical properties, the stress-strain relationship of expansive soil changed from strain softening to strain hardening by adding two kinds of OSP, and the influence on pore pressure strain relationship also had obvious regularity. Compared with plain soil, the effective cohesion of ESMO ($d_{osp} < 0.075$ mm) and ESMO ($d_{osp} < 1$ mm) increased by 32.8 % and 15.4 %, respectively.
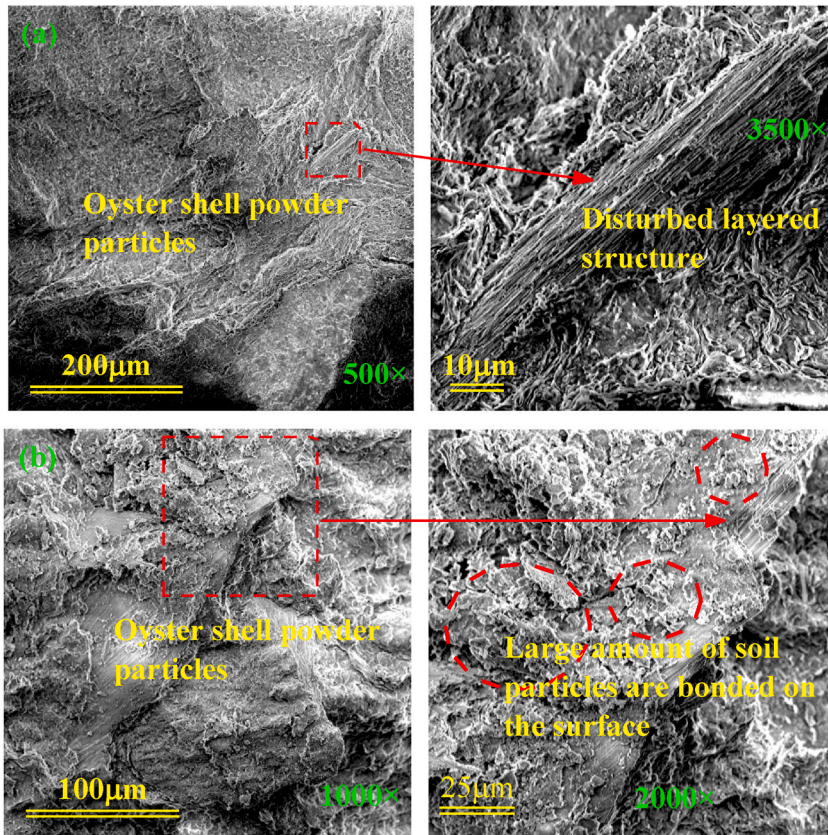
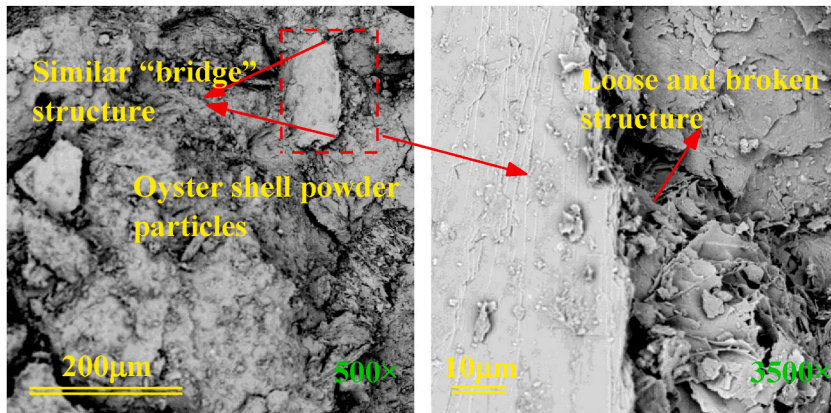**Fig. 19.** Layered structure of disturbance.

Fig. 20. Loose and broken structure.

(2) Under long-term cyclic loading, the cumulative plastic strain of ESMO (d_{osp} < 0.075 mm) is 40.2 % lower than that of plain soil, and the cumulative velocity and stability value of pore water pressure are also slightly reduced, the energy dissipation capacity is reduced, and the stiffness is increased. The performance of ESMO (d_{osp} < 1 mm) is completely opposite. Therefore, when the content is 9 %, the dynamic performance of ESMO can be major improved by controlling the particle size of OSP below 0.075 mm.

(3) Mechanical occlusion, filling effect and cementation of calcium carbonate are essential reasons for improving the mechanical performance of ESMO. The selection of OSP with appropriate particle size is the key to improving the strength of modified soil. Physical and chemical changes may affect the interaction between OSP and expansive soil. For example, the change of trace

calcium ions precipitated from calcium carbonate in water and the pH of pore water may cause the change of expansive soil properties. This provides a direction for future research.

Funding

Data availability

Data generated and analysed during the current study are available from the corresponding author on reasonable request.

CRediT authorship contribution statement

Wencan Jiao: Writing – review & editing, Project administration, Methodology, Funding acquisition, Formal analysis, Data curation. **Weizheng Zhou:** Writing – original draft, Validation, Methodology, Investigation, Data curation. **Zhen Huang:** Writing – review & editing, Methodology, Investigation, Funding acquisition, Formal analysis, Data curation, Conceptualization. **Riyan Lan:** Writing – review & editing, Resources, Investigation. **Min Ma:** Validation, Data curation.

Declaration of competing interest

The author(s) declared no potential conflicts of interest with respect to the research, authorship, and/or publication of this article.

References

[1] H.P. Yang, J. Wang, W.T. Zhan, Study of treatment technology and design scheme of expansive soil subgrade for Nanning outer ring expressway, Rock Soil Mech. 32 (S2) (2011) 359–365, https://doi.org/10.16285/j.rsm.2011.s2.057.

[2] H. Yang, L. Lin, Y. He, Soil erosion caused by highway construction in expansive soils districts and its prevention measures, in: Geotechnical Engineering for Disaster Mitigation and Rehabilitation: Proceedings of the 2nd International Conference GEDMAR08, 2008, pp. 781–789, https://doi.org/10.1007/978-3-540-79846-0_100.

[3] A. Al-Taie, M. Disfani, R. Evans, A. Arulrajah, S. Horpibulsuk, Volumetric behavior and soil water characteristic curve of untreated and lime-stabilized reactive clay, Int. J. GeoMech. 19 (2) (2019) 04018192, https://doi.org/10.1061/(ASCE)GM.1943-5622.0001336.

[4] A.A.B. Moghal, B.C. Chittoori, B.M. Basha, Effect of fibre reinforcement on CBR behaviour of lime-blended expansive soils: reliability approach, Road Mater. Pavement Des. 19 (3) (2018) 690–709, https://doi.org/10.1080/14680629.2016.1272479.

[5] G. Parvathy, et al., Understanding the impact of lime stabilization on expansive soil for grounding and analysis adopting LIBS, IEEE Access 10 (2022) 21066–21076, https://doi.org/10.1109/ACCESS.2022.3149338.

[6] J. Du, A. Zhou, X. Lin, Y. Bu, J. Kodikara, Revealing expansion mechanism of cement-stabilized expansive soil with different interlayer cations through molecular dynamics simulations, J. Phys. Chem. C 124 (27) (2020) 14672–14684, https://doi.org/10.1021/acs.jpcc.0c03376.

[7] P.S.K. Raja, T. Thyagaraj, Significance of compaction time delay on compaction and strength characteristics of sulfate resistant cement-treated expansive soil, J. Rock Mech. Geotech. Eng. 13 (5) (2021) 1193–1202, https://doi.org/10.1016/j.jrmge.2021.03.003.

[8] V.N. Mypati, S. Saride, Feasibility of alkali-activated low-calcium fly ash as a binder for deep soil mixing, J. Mater. Civ. Eng. 34 (1) (2022) 04021410, https://doi.org/10.1061/(ASCE)MT.1943-5533.0004047.

[9] J. Pooni, D. Robert, C. Gunasekara, F. Giustozzi, S. Setunge, Mechanism of enzyme stabilization for expansive soils using mechanical and microstructural investigation, Int. J. GeoMech. 21 (10) (2021) 04021191, https://doi.org/10.1061/(ASCE)GM.1943-5622.0002164.

[10] S. Arefin, H. Al-Dakheeli, R. Bulut, Stabilization of expansive soils using ionic stabilizer, Bull. Eng. Geol. Environ. 80 (2021) 4025–4033, https://doi.org/10.1007/s10064-021-02179-5.

[11] X.S. Zhuang, J. Wang, K. Wang, K. Li, Z. Hu, Experimental study on dynamic characteristics of expansive soil modified by weathered sand, Rock Soil Mech. 39 (S2) (2018) 149–156, https://doi.org/10.16285/j.rsm.2018.1241.

[12] X.S. Zhuang, J.X. Wang, K. Li, K. Wang, Z. Hu, Comparative study on characteristic of hysteretic curves of expansive soil improved by weathered sand, Chin. J. Rock Mech. Eng. 38 (S2) (2019) 3709–3716, https://doi.org/10.13722/j.cnki.jrme.2018.1375.

[13] Y.Z. Xu, Z.Q. Huang, C. Su, R.K. Yan, Study on the influence of modified width of gravel on lateral swelling force of expansive soil, J. Railw. Sci. Eng. 18 (6) (2021) 1456–1463, https://doi.org/10.19713/j.cnki.43-1423/u.T20200714.

[14] J.K. Mitchell, J.C. Santamarina, Biological considerations in geotechnical engineering, J. Geotech. Geoenviron. Eng. 131 (10) (2005) 1222–1233.

[15] Z. Huang, H.Y. Sun, Y.M. Dai, P.B. Hou, W.Z. Zhou, L.L. Bian, A study on the shear strength and dry-wet cracking behaviour of waste fibre-reinforced expansive soil, Case Stud. Constr. Mater. 16 (2022) e01142, https://doi.org/10.1016/j.cscm.2022.e01142.

[16] M. Syed, A. GuhaRay, Effect of natural fiber reinforcement on strength response of alkali activated binder treated expansive soil: experimental investigation and reliability analysis, Construct. Build. Mater. 273 (2021) 121743, https://doi.org/10.1016/j.conbuildmat.2020.121743.

[17] J. James, P.K. Pandian, Bagasse ash as an auxiliary additive to lime stabilization of an expansive soil: strength and microstructural investigation, Adv. Civ. Eng. 2018 (2018) 9658639, https://doi.org/10.1155/2018/9658639.

[18] M.K. Atahu, F. Saathoff, A. Gebissa, Strength and compressibility behaviors of expansive soil treated with coffee husk ash, J. Rock Mech. Geotech. Eng. 11 (2) (2019) 337–348, https://doi.org/10.1016/j.jrmge.2018.11.004.

[19] J. Ma, Y. Su, Y. Liu, X. Tao, Strength and microfabric of expansive soil improved with rice husk ash and lime, Adv. Civ. Eng. 2020 (2020) 9646205, https://doi.org/10.1155/2020/9646205.

[20] Fishery Administration Bureau of Ministry of Agriculture and Rural Affairs, National Fisheries Technology Extension Station, Chinese Fisheries Association, 2020 Chinese Fishery Statistical Yearbook, China Agriculture Press, Beijing, 2020.

[21] M. Lu, et al., Modification of oyster shell powder by humic acid for ammonium removal from aqueous solutions and nutrient retention in soil, J. Environ. Chem. Eng. 9 (6) (2021) 106708, https://doi.org/10.1016/j.jece.2021.106708.

[22] K. You, et al., Lanthanum-modified magnetic oyster shell and its use for enhancing phosphate removal from water, Colloids Surf. A Physicochem. Eng. Asp. 633 (2022) 127897, https://doi.org/10.1016/j.colsurfa.2021.127897.

[23] Y. Chen, J. Xu, Z. Lv, L. Huang, J. Jiang, Impacts of biochar and oyster shells waste on the immobilization of arsenic in highly contaminated soils, J. Environ. Manag. 217 (2018) 646–653, https://doi.org/10.1016/j.jenvman.2018.04.007.

[24] L.R.S. Andrade, et al., Oyster shell-based alkalinization and photocatalytic removal of cyanide as low-cost stabilization approaches for enhanced biogas production from cassava starch wastewater, Process Saf. Environ. Protect. 139 (2020) 47–59, https://doi.org/10.1016/j.psep.2020.04.008.

[25] Y. Liao, et al., Influence of the usage of waste oyster shell powder on mechanical properties and durability of mortar, Adv. Powder Technol. 33 (3) (2022) 103503, https://doi.org/10.1016/j.apt.2022.103503.

[26] Z. Chen, et al., Experimental study on the shear performance of brick masonry strengthened with modified oyster shell ash mortar, Case Stud. Constr. Mater. 13 (2020) e00469, https://doi.org/10.1016/j.cscm.2020.e00469.

[27] N.N.H. Tri, P.N.H. Huong, H.T. Van, S.N. Khanh, A study on the applicability of microbially induced calcium carbonate precipitation on soil-sand stabilization through the bio-cementation process, IOP Conf. Ser. Earth Environ. Sci. 1226 (2023) 012028, https://doi.org/10.1088/1755-1315/1226/1/012028.

[28] X.S. Zhuang, T. Zhuang, G.L. Tao, H.W. Zhao, W.X. Li, Experimental study on dynamic deformation and dynamic strength of expansive soil modified by phosphorus tailings, Chin. J. Rock Mech. Eng. 39 (S1) (2020) 3032–3038, https://doi.org/10.13722/j.cnki.jrme.2019.0776.

[29] X.S. Zhuang, et al., Experimental study of dynamic elastic modulus and damping ratio of improved expansive soil under cyclic loading by expanded polystyrene, Rock Soil Mech. 42 (9) (2021) 2427–2436, https://doi.org/10.16285/j.rsm.2021.0061.

[30] Z. Huang, L.L. Bian, Y. Liu, W.Z. Zhou, S.K. Ma, Study on engineering characteristics and microscopic mechanism of expansive soil improved by oyster shell powder, J. Railw. Sci. Eng. 20 (5) (2023) 1729–1739, https://doi.org/10.19713/j.cnki.43-1423/u.t20220987.

[31] Z. Huang, B. Gong, W.C. Jiao, W.Z. Zhou, Y. Shao, S.K. Ma, Dynamic behaviour of oyster shell powder-modified expansive soil under cyclic loading, Construct. Build. Mater. 409 (2023) 134133, https://doi.org/10.1016/j.conbuildmat.2023.134133.

[32] Ministry of Water Resources of the People's Republic of China, Standard for Geotechnical Testing Method (GBT 50123-2019), China Planning Press, Beijing, 2019.

[33] Ministry of Housing and Urban-Rural Development of the People's Republic of China, Technical Code for Buildings in Expansive Soil Regions (GB 50112-2013), China Architecture & Building Press, Beijing, 2012.

[34] Z. Zeng, H. Lu, Y. Zhao, Y. Qin, Analysis of the mineral compositions of swell-shrink clays from Guangxi province, China, Clay Clay Miner. 68 (2020) 161–174, https://doi.org/10.1007/s42860-019-00056-7.

[35] W.T. Chen, Study on Component, Properties of Oyster Shell and its Recycling, Fujian Agriculture and Forestry University, 2013, 2013.

[36] D. Li, S. Zhang, The influences of sand content and particle size on the desiccation cracks of compacted expansive soil, Adv. Mater. Sci. Eng. 2021 (2021) 7752352, https://doi.org/10.1155/2021/7752352.

[37] H.M. Mohamad, et al., Maximum strain effect and secant modulus variation of hemic peat soil at large deformation due to cyclic loading, Civil Eng. J. 8 (10) (2022) 2243–2260, https://doi.org/10.28991/CEJ-2022-08-10-015.

[38] T. Zhang, Experiment Study on Dynamic Characteristics of Remolded Clay with Different Consolidation Degree under Subway Loading, Zhejiang University, 2014, 2014.

[39] B.W. Kong, Z. Ding, S.H. He, J.H. Zhuang, Experimental study on pore features and dynamic behaviors of soft clay under different confine pressures during freezing, Chin. J. Rock Mech. Eng. 39 (11) (2020) 2328–2340, https://doi.org/10.13722/j.cnki.jrme.2020.0496.

[40] Z. Ding, et al., Study on pore pressure and microstructure of frozen and thawed soft soil under subway cyclic loading, Chin. J. Rock Mech. Eng. 35 (2016) 2328–2336, https://doi.org/10.13722/j.cnki.jrme.2015.1620.

[41] M. Wang, Z. Shan, Y. Wang, S. Di, Dynamic elastic moduli and damping ratios of marine sediments at Zhoushan Daishan based on dynamic triaxial tests under strain control, Chin. J. Rock Mech. Eng. 33 (7) (2014) 1503–1512, https://doi.org/10.13722/j.cnki.jrme.2014.07.024.

[42] A.E. Amaludin, et al., Physicochemical and microstructural characterization of Klias peat, Lumadan POFA, and GGBFS for geopolymer based soil stabilization, HighTech and Innov. J. 4 (2) (2023) 327–348, https://doi.org/10.28991/HIJ-2023-04-02-07.

[43] P.R. Rangan, et al., Assessment of fly ash-rice straw ash-laterite soil based geopolymer mortar durability, Civil Eng. J. 9 (6) (2023) 1456–1470, https://doi.org/10.28991/CEJ-2023-09-06-012.